Causes of Ionization in Rocket Exhausts

L. Douglas Smoot*
Brigham Young University, Provo, Utah

Forty-nine radar attenuation tests at *X*-band frequency were made using 1 lb solid propellant charges in an altitude facility at ambient pressures of 280 and 140 mm Hg. Transverse attenuation was measured along the exhaust plume, using a moving microwave cart. Propellant aluminum level, solids loading level, and potassium impurity level were systematically varied. Tests were conducted in nitrogen and air atmospheres. Results of these tests were compared with predicted attenuation levels which were based on equilibrium thermal ionization of the alkali metal during afterburning of plume and ambient air. Microwave attenuation predictions considered a line-of-sight ray traversing a series of uniform sections of the ionized plume. Agreement of predicted and measured peak attenuation levels was excellent for a wide range of propellant formulations, providing evidence as to the causes of ionization.

Introduction

PREVIOUS work[1-4] has provided an indication of possible causes of ionization in solid propellant rocket exhausts. The work of Wood and DeMore[3] has demonstrated the significance of thermal ionization of alkali metal impurities during afterburning of the exhaust plume and ambient air. Capener, et al.[2] measured influences of ambient pressure and aluminum level on exit plane electron density. Methods for predicting plume ionization for equilibrium[1,5,6] and nonequilibrium plumes[4] have been presented. In addition, available techniques[7,8] for estimating the attenuation of a microwave signal traversing an ionized plume have been reported. This paper reports the results of a series of comprehensive measurements wherein effects of propellant formulation, alkali metal level, ambient composition, and pressure on radar attenuation were measured and compared with predicted values. Results establish dominant causes of attenuation and also provide important trade-off data not previously available for selection of propellants with specified ionization levels.

Experimental

Test Motor and Facility

The small test motor contained 1 lb of solid propellant, cast as an end burning grain; operating chamber pressure was approximately 1200 psia while the 15° conical graphite nozzle had a throat diameter of 0.18 in. and an expansion ratio of 9.3. The motor produced a thrust of approximately 50 lb_f for 4 sec. The motor was mounted inside the Naval Research Laboratory test chamber (6' × 7' × 10') equipped with steam jet ejectors for maintaining the test pressure. Focused *X*-band (10 Ghz) microwave horns were mounted perpendicularly to the motor axis and 12 in. apart on a moving sled. During each test firing, the microwave horns traversed along the exhaust plume length and normal to it at least twice. Test cell pressure, motor chamber pressure, and *X*-band attenuation were monitored during the test run.

Test Program and Results

Thirty-two tests in an ambient air atmosphere were conducted at a near constant ambient pressure of 280mm Hg, corresponding to a simulated attitude of 25,000 ft. An additional 13 tests were conducted at an ambient pressure of 140 mm Hg corresponding to a simulated test altitude of 40,000 ft. Tests were conducted using typical rubber base propellants containing ammonium perchlorate (AP) oxidizer. Aluminum level was varied from 4 to 20% for two separate solids loading levels† of 84 and 88%. The propellant potassium level was systematically varied over three orders of magnitude from 10 ppm to 10,000 ppm. Impurity levels were established using a flame photometer. Peak attenuation levels in the afterburning regions of the plume are summarized in Figs. 1 and 2 where effect of aluminum level is illustrated. Peak attenuation values occurred from 12 to 20 in. aft of the nozzle exit plane, with the farther aft-distances more prevalent at the lower ambient test pressures. Attenuation was observed to increase significantly with increasing aluminum level for each of solids loading levels tested. The increase in attenuation with increasing aluminum level was greatest at the higher solids loading levels.

These same data are replotted in Figs. 3 and 4 to illustrate the effect of potassium impurity at both test cell pressures. Attenuation for all propellant systems tested varied approximately as the square root of the alkali metal level for the higher air pressure conditions tested, with somewhat increased dependence at the lower pressure. Only two air pressures, corresponding to two test altitudes, were tested: 25,000 ft (280 mm Hg) and 40,000 ft (140 mm Hg). The data generally show lower peak attenuation levels at the higher altitudes, especially for the lower solids loading levels. The peak attenuation levels occurred farther aft of the nozzle exit plane for all tests at the higher altitude.

An additional 4 tests were conducted in a nitrogen atmosphere but only insignificant levels of attenuation were measured in these cases. In the presence of nitrogen, the attenuation measured in the afterburning regions of the exhaust plume was completely suppressed.

Attenuation Predictions

Controlling Processes

For tests previously reported and in Ref. 3 in a static air atmosphere, attenuation was highly dependent upon the alkali metal level in the propellants. This indicates that thermal ionization is an important and probably dominant mechanism of electron production for the test conditions and propellants investigated.

Attenuation levels were greatly reduced or eliminated when motors were tested in the presence of nitrogen, when com-

Received May 15, 1974; revision received November 4, 1974. This work was sponsored by the Naval Air Systems Command, Washington D.C. The assistance of M. R. King and G. Cann of the Lockheed Propulsion Company and H. Merchant and W. W. Balwanz of the Naval Research Laboratories is acknowledged.

Index categories: Jets, Wakes and Viscid-Inviscid Flow Interactions; Plasma Dynamics and MHD; Thermochemistry and Chemical Kinetics.

*Professor and Chairman, Chemical Engineering. Member AIAA.

†Percent solids loading is defined as (% AP + % Al). The balance of the propellant is binder, which was a carboxy-terminated polybutadiene polymer containing small percentages of curatives.

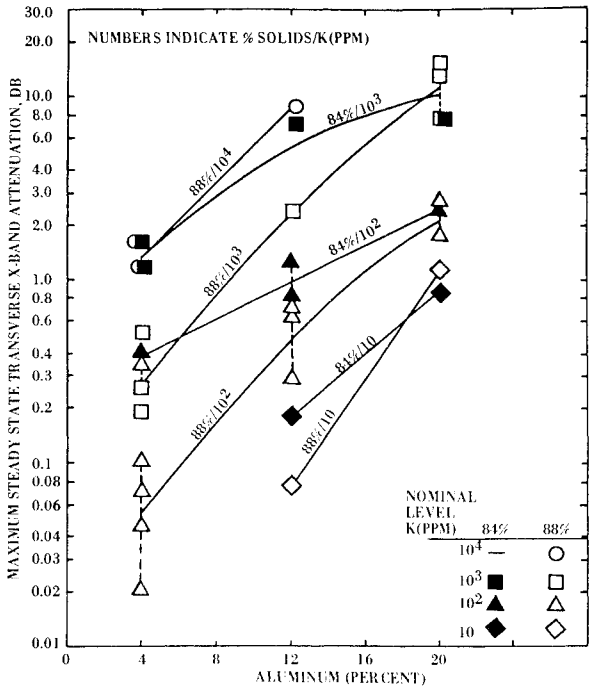

Fig. 1 Effect of aluminum, solids loading, and alkali metal level on X-band radar attenuation at 280 mm Hg ambient pressure.

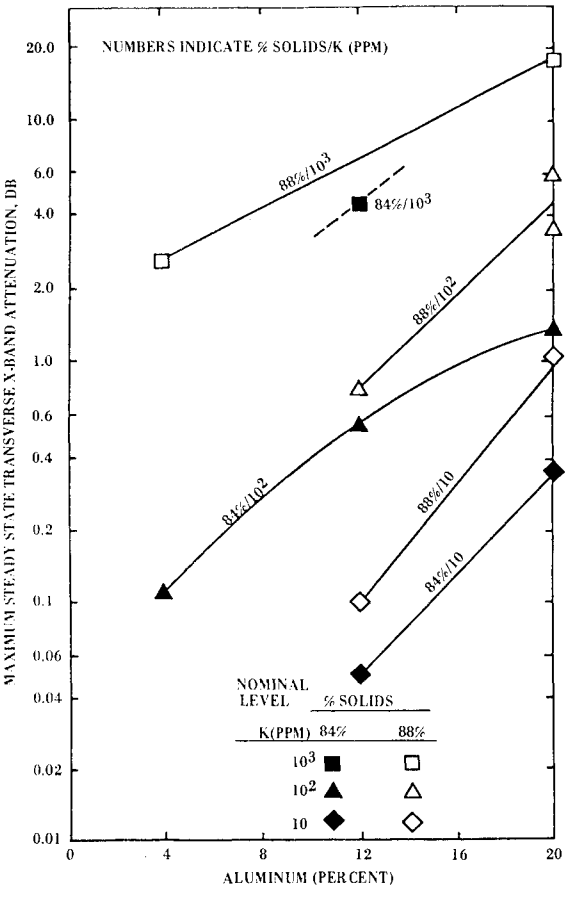

Fig. 2 Effect of aluminum, solids loading, and alkali metal level on X-band radar attenuation at 140 mm Hg ambient pressure.

pared with tests in air, indicating that plume-air mixing and subsequent combustion is a major cause of radar attenuation. Attenuation resulting from residual chamber ionization did not appear to be a major contributor to the attenuation level.

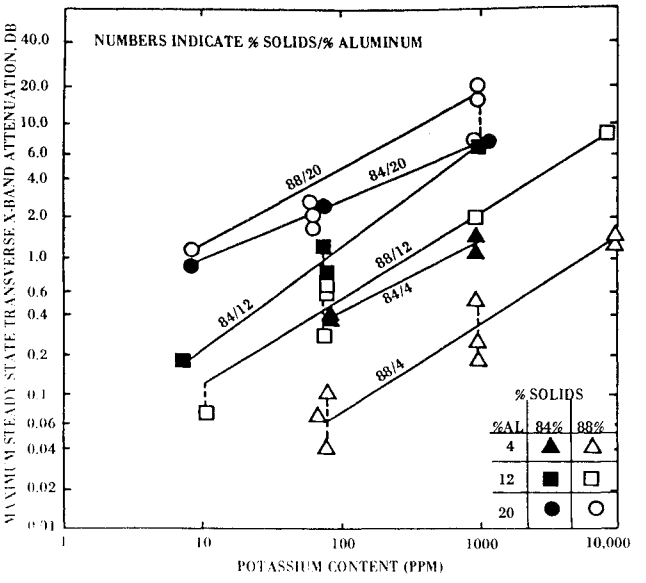

Fig. 3 Effect of alkali metal level on maximum X-band attenuation for various propellant formulations in air at 280 mm Hg ambient pressure.

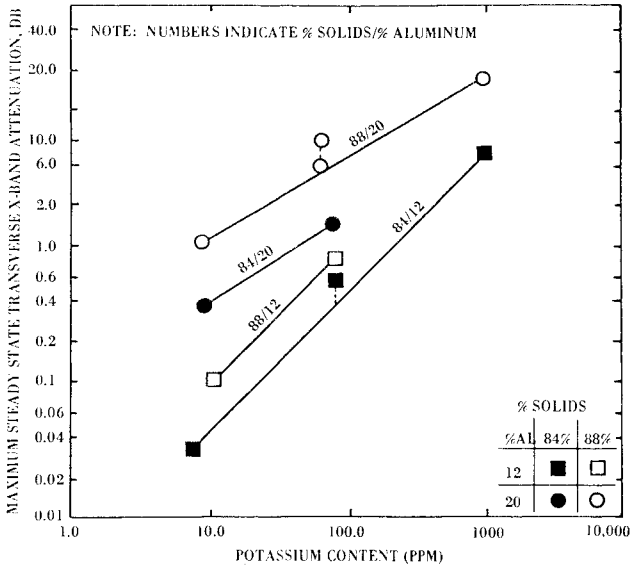

Fig. 4 Effect of alkali metal level on maximum X-band attenuation for various propellant formulations in air at 140 mm Hg ambient ambient pressure.

Regions very near the nozzle were not explored in this study, nor were very high altitude regions where plume-air afterburning may not occur. These results strongly indicate that the thermal ionization of alkali metal impurities occurring during afterburning of the plume and air is the predominant cause. This result appears to be applicable to the entire range of propellants investigated, and up to altitudes of at least 40,000 ft. The attenuation model presented following is based on this process.

Plume-Air Mixing and Afterburning Model

The model developed by Donaldson and Gray[6] for characterizing the turbulent mixing of an axisymmetric free jet with a quiescent stream was extended to include influences of a moving secondary stream.[5] However, in neither of these cases were the effects of combustion of the two streams treated. The technique for extending this basic approach to treat reacting gas mixtures in equilibrium is summarized briefly.

For a steady, axisymmetric, turbulent, compressible free jet reacting with a secondary stream, it has been shown[9] for the case of unity turbulent Schmidt and Prandtl numbers and uniform pressure, that the following similarity relations are applicable:

$$(y_i - y_{i\infty})/(y_{il} - y_{i\infty}) = (u - u_\infty)/(u_l - u_\infty) = (h^\circ - h^\circ_\infty)/(h^\circ_l - h^\circ_\infty) \quad (1)$$

where y is the mass fraction of the i^{th} element, u is the axial velocity, h° is the stagnation enthalpy and the subscripts (1) and (∞) refer to exit jet and freestream conditions, respectively. Equation (1) is general for a multi-component, reacting-gas mixture and applies to frozen, equilibrium, or nonequilibrium situations.

From Eq. (1), for any assumed value of velocity u, values for h°, y_i and $h = h^\circ - u^2/2$ can be computed. The complete chemical equilibrium information is obtained[10] as a function of velocity, including electron density, ion densities, major specie composition, etc. The dependence of gas density on velocity determined in this manner for a representative solid propellant is shown in Fig. 5.

For the case of mixing of a jet and air without combustion, the density ratio, ρ/ρ_∞, as a function of reduced velocity was formally given by the expression[5,6]:

$$\rho/\rho_\infty = (P\,U' + 1)/(MU' + 1)[1 + A'U' - B'(U')^2] \quad (2)$$

where $U' = (u - u_\infty)/(u_l - u_\infty)$, $M = (m_\infty/m_l) - 1$, m is the molecular weight. Equation (2) corresponds to the upper curve of Fig. 5.

For the case with simultaneous mixing and burning of interest here, no such explicit theoretical function can be developed to predict the lower curve of Fig. 5. However, it may often be assumed for the case with simultaneous mixing and burning that the form of Eq. (2) still applies, but where the theoretically established constants P, A', and B' are replaced by empirically evaluated constants using ρ/ρ_∞ vs U' data from a general thermochemical equilibrium program.[10] Therefore, for the case with simultaneous mixing and burning:

$$\rho/\rho_\infty = (C_1U' + 1)/(MU' + 1)[1 + C_2U' - C_3(U')^2] \quad (3)$$

The success of Eq. (3) in describing the density vs velocity relationship is shown in Fig. 5 where the lower solid line drawn through the data points was obtained from this correlative equation. Agreement between density values from

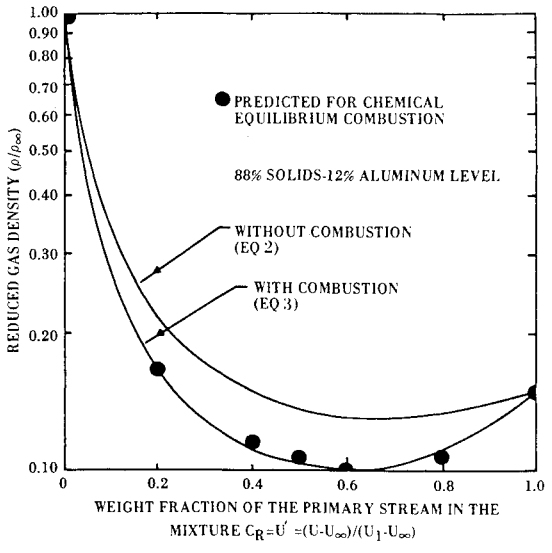

Fig. 5 Variation of gas density with weight fraction of air in a plume-air mixture.

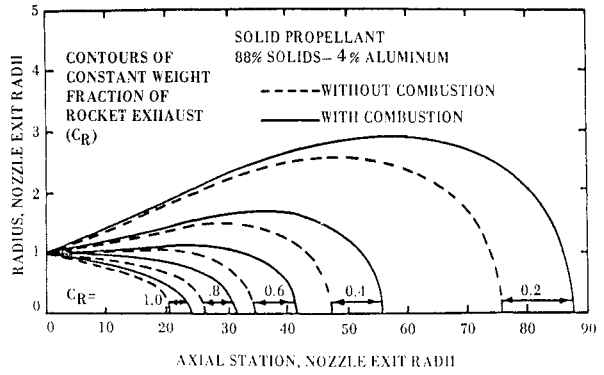

Fig. 6 Effect of afterburning on predicted plume structure.

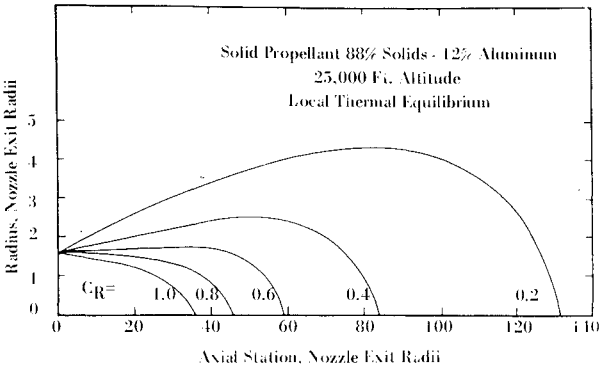

Fig. 7 Predicted exhaust plume structure for solid propellant exhaust at 280 mm Hg ambient pressure.

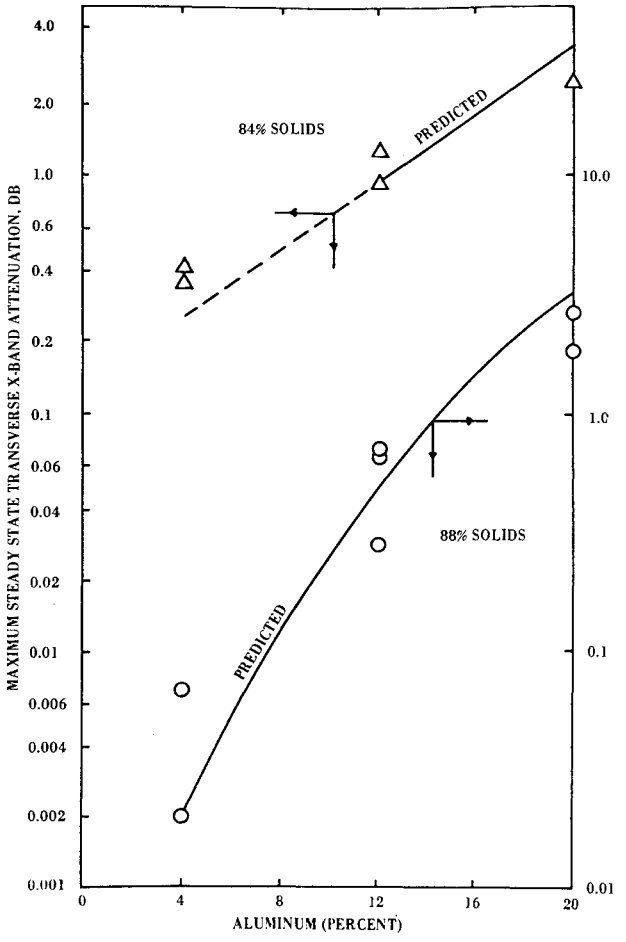

Fig. 8 Comparison of the predicted and measured effect of aluminum and solids loading levels on radar attenuation (X-band) at 280 mm Hg ambient pressure.

Table 1 Summary of selected predicted plume properties for a typical solid propellant system (see Fig. 7)[a] 88% solids—12% aluminum

Property	Weight fraction of exhaust 0.0	0.2	0.4	0.6	0.8	1.0
Static temp. (K)	238.0	1765.0	2401.0	2500.0	2291.0	1697.0
Electron density (e^-/cc)[b]	0.0	5.6^{5}	1.2^{10}	5.4^{10}	1.3^{10}	9.4^{6}
Velocity	0.0	1840.0	3681.0	5521.0	7361.0	9202.0
Density (lb/ft^3)	3.5^{-2}	4.6^{-3}	3.3^{-3}	3.0^{-3}	3.0^{-3}	3.7^{-3}
Molecular weight of gas	29.0	28.7	28.0	26.5	24.5	22.3
Heat capacity (Btu/lb°R)	0.24	0.32	0.36	0.39	0.41	0.42
Composition[c] (Mols/100g)						
Total gas	3.45	3.32	3.24	3.25	3.34	3.46
CO	0.0	1.1^{-4}	4.9^{-2}	0.24	0.48	0.66
CO_2	0.0	0.17	0.30	0.28	0.21	0.21
H_2O	0.0	0.33	0.63	0.85	0.92	0.85
HCl	0.0	0.12	0.21	0.34	0.50	0.65
N_2	2.73	2.25	1.76	1.28	0.81	0.33
H_2	0.0	6.0^{-5}	1.8^{-2}	0.12	0.37	0.77
e^-	0.0	0.12^{-11}	0.35^{-7}	0.16^{-6}	0.35^{-7}	0.20^{-10}

[a] For exhaust plume ideally expanded to static pressure of 5.5 psia at 25,000 ft altitude.
[b] $5.6^{5} = 5.6 \times 10^{5}$, etc.
[c] Only selected major species are shown, together with electron concentration.

Table 2 Thermochemical equilibrium properties of propellant exhausts[a]

Percent solids[b]	88.0	88.0	88.0	88.0	88.0	88.0	84.0	84.0
Aluminum level (wt%)	4.0	12.0	12.0	12.0	12.0	20.0	12.0	20.0
Potassium level (ppm)	58.0	10.0	59.0	1059.0	9888.0	59.0	62.0	58.0
P_c (psia)	1200.0	1200.0	1200.0	1200.0	1200.0	1200.0	1200.0	1200.0
T_c (K)	3185.0	3437.0	3437.0	3434.0	3408.0	3625.0	3138.0	3250.0
Expansion ratio	9.34	9.34	9.34	9.34	9.34	9.34	9.34	9.34
T_e, frozen (K)	1457.0	1667.0	1667.0	1666.0	1653.0	1835.0	1429.0	1536.0
T_e, equilibrium (K)	1702.0	2080.0	2080.0	2076.0	2045.0	2317.0	1661.0	2001.0
U_e (fps)	8242.0	8378.0	8378.0	8368.0	8285.0	8446.0	8329.0	8357.0
Exit e-/cc frozen[c]	1.3^{11}	2.2^{11}	7.2^{11}	2.4^{12}	6.6^{12}	2.1^{11}	3.7^{10}	3.6^{10}
Exit e-/cc equilibrium	6.3^{6}	6.8^{8}	1.8^{9}	6.7^{9}	6.8^{10}	2.9^{10}	6.9^{6}	1.6^{9}
Exit pressure (psia)	17.0	19.1	19.1	19.0	18.9		17.2	19.5
Exit-plane equilibrium properties (g moles/100 g)								
Moles gas	3.67	3.46	3.46	3.46	3.42	3.27	3.87	3.66
Cl	2.4^{-4}	2.5^{-3}	2.5^{-3}	2.4^{-3}	2.0^{-3}	6.2^{-3}	7.9^{-5}	6.7^{-4}
CO	0.43	0.69	0.69	0.69	0.68	0.83	1.03	1.16
CO_2	0.44	0.17	0.17	0.17	0.17	3.8^{-2}	0.22	0.34
HCT	0.71	0.64	0.64	0.64	0.63	0.57	0.61	0.43
H_2	0.39	0.73	0.73	0.73	0.72	1.21	1.27	1.73
H_2O	1.34	0.88	0.88	0.88	0.87	0.31	0.51	3.5^{-3}
N_2	0.36	0.33	0.33	0.33	0.32	0.29	0.31	0.28
A_2O_3(c)	7.4^{-2}	0.22	0.22	0.22	0.22	4.8^{-6}	0.22	0.34
K	1.1^{-8}	4.0^{-8}	2.4^{-7}	4.2^{-6}	3.3^{-5}	1.1^{-6}	1.8^{-8}	3.4^{-7}
K^+	4.2^{-8}	4.0^{-7}	9.1^{-7}	4.1^{-6}	1.0^{-5}	3.7^{-6}	1.0^{-8}	5.4^{-7}
KCl	1.5^{-4}	2.5^{-5}	1.5^{-4}	2.7^{-3}	2.5^{-2}	1.5^{-4}	1.8^{-5}	1.5^{-4}
Na	1.9^{-7}	1.1^{-7}	3.8^{-6}	3.7^{-6}	3.1^{-6}	1.4^{-5}	9.8^{-9}	4.7^{-6}
Na^+	3.0^{-9}	1.3^{-8}	1.7^{-7}	4.2^{-8}	1.0^{-8}	8.8^{-7}	3.9^{-10}	7.2^{-8}
NaCl	6.3^{-4}	2.1^{-5}	7.3^{-4}	7.3^{-4}	7.3^{-4}	6.3^{-4}	2.2^{-5}	6.1^{-4}
Cl^-	4.5^{-8}	4.2^{-7}	1.1^{-6}	4.1^{-6}	1.0^{-5}	4.6^{-6}	1.0^{-8}	6.1^{-7}

[a] Exponent shown is power of 10, i.e., $1.3^{11} = 1.3 \times 10^{11}$.
[b] Percent solids = percent ammonium perchlorate + percent aluminum.
[c] Assumes no chemical reaction in nozzle. Mole fractions frozen at chamber values.

the correlation and from the thermochemical equilibrium program is often adequate. When the form of Eq. (3) is not adequate, numerical techniques have been used to improve accuracy.[11]

With a functional relationship between density and velocity, the equations of continuity and motion can be solved to give velocity as a function of axial and radial position in the plume. For the case where Eq. (3) is used, the solution is identical to that of Donaldson and Gray[6] for quiescent air and that of Smoot and Purcell[5] for moving air.

Predictions of exhaust plume structure for both frozen and equilibrium jets were made for the solid propellant shown in Fig. 6. The particles have been assumed to be in dynamic equilibrium with the gases and to have mass but no volume, thus influencing the gas density. Contour lines of Fig. 6 are weight fractions of the rocket exhaust (Cr) in the exhaust/air mixture. For each weight fraction, a unique set of values of velocity, electron density, temperature, and composition exist. The solid lines resulted from the equilibrium model which treats simultaneous mixing and afterburning while the

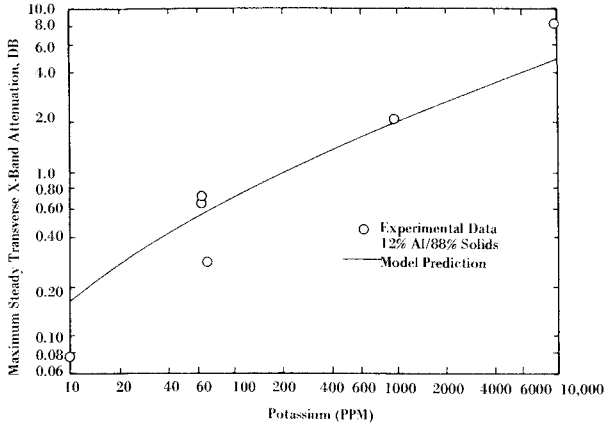

Fig. 9 Comparison of the predicted and measured effect of alkali metal level on radar attenuation (*X*-band) at 280 mm Hg ambient pressure.

dashed lines are predictions for the nonreactive plumes. This difference is even more pronounced for more fuel-rich solid propellant systems. Model predictions for a second system at 280 mm Hg ambient pressure are shown in Fig. 7, assuming thermal equilibrium. Table 1 provides additional properties for each weight fraction contour line. Equilibrium ionization levels near the exit plane are low compared to values in the afterburning regions. In Fig. 7, the contours begin at a radial dimension that is larger than the actual nozzle radius because the jet has been expanded to the ambient pressure.

Attenuation Predictions and Comparison with Measurements

With the exhaust plume structure previously deduced including electron density, temperature, and species distributions, collision cross section, and microwave attenuation are readily computed for any path through the plume using available techniques and data.[7,8] The nonuniform plume is divided into a series of uniform concentric annuli.

Thermochemical calculations, exhaust plume descriptions, and attenuation predictions have been made for systems corresponding to eight selected cases which were considered experimentally. Thermochemical properties of these systems are summarized in Table 2. Predictions of peak attenuation levels are compared with experimental values in Figs. 8 and 9. Figure 8 compares predicted and measured influences of aluminum and solids loading levels. Agreement is excellent. Increasing aluminum level causes the attenuation level to increase by producing a more fuel-rich, hotter, more ionized exhaust gas, while decreasing solids loading level at constant aluminum level causes increases in the rubber level and decreases AP level. These changes decrease electron attachment to Cl and formation of KCl while substantially increasing afterburning potential. Comparison of predicted and measured effects of potassium level is shown in Fig. 9 for a single propellant system. Agreement of theory and experiment is remarkable considering the complexity of the process.

While equilibrium theory has been adequate for this set of test conditions, there is theoretical evidence[12] that nonequilibrium effects become important at lower ambient pressures, corresponding to an altitude of less than 50,000 ft for conditions considered in that reference. This nonequilibrium effect may be altered significantly by inviscid plume and air shock effects which were not considered in Ref. 12.

Conclusions

Ionization level and attenuation increase strongly with increasing aluminum level and generally with decreasing solids-loading level. However, higher solids-loading levels were of little advantage at the highest aluminum levels. Attenuation varied approximately as the square root of the potassium level for the ambient pressures tested.

Causes of radar attenuation in rubber-base solid propellant micromotors were characterized for a range of propellants. Thermal ionization of alkali metal impurity occurring during afterburning of plume and air was sufficient to account for the observed attenuation.

Predicted peak attenuation levels using a model based on equilibrium thermal ionization of alkali metals during plume-air afterburning were remarkably precise when considering the limitations in forming a physical description of the processes occurring. The model accurately predicted the dependence of aluminum level, solids-loading level, and alkali metal level, implying that thermal equilibrium exists for these test conditions to an altitude of 40,000 ft.

References

[1] Smoot, L. D. and Underwood, D. L., "Prediction of Microwave Attenuation Characteristics of Rocket Exhausts," *Journal of Spacecraft and Rockets,* Vol. 3, March 1966, pp. 302-309.

[2] Capener, E. L., Chawn, J. B., Dickinson, L. A., and Nonevicz, J. E., "Studies on Ionization Phenomena Associated with Solid Propellant Rockets," *AIAA Journal,* Vol. 4, Aug. 1966, pp. 1349-1354.

[3] Wood, W. A. and DeMore, J. E., "Microwave Attenuation Characteristics of Solid Propellant Rocket Exhaust Products," AIAA Paper 65-183, 1965, Washington, D.C.

[4] Pergament, H. S. and Calcote, H. E., "Thermal and Chemi-Ionization Processes in Afterburning Rocket Exhausts," *Eleventh Symposium (International) on Combustion,* The Combustion Institute, 1967, Pittsburgh, Pa.,p. 597.

[5] Smoot, L. D. and Purcell, W. E., "Mixing of a Compressible Free Jet With a Moving Environment," *AIAA Journal,* Vol. 5, Nov. 1967, pp. 2049-2052.

[6] Donaldson, C. duP and Gray, K. E., "Theoretical and Experimental Investigation of the Compressible Free Mixing of Two Dissimilar Gases," *AIAA Journal,* Vol. 4, Nov. 1966, pp. 2017-2025.

[7] Molmud, P., "The Electrical Conductivity of Weakly Ionized Gases," Paper 2586-62, American Rocket Society, 1962.

[8] Balwanz, W. W. and Weston, J. P., "The Prediction of Rocket Exhaust Interference with Radio Signals," Paper 2591-62 American Rocket Society, 1962.

[9] Libby, P. A., "Theoretical Analysis of Turbulent Mixing of Reactive Gases with Application to Supersonic Combustion of Hydrogen," *ARS Journal,* Vol. 32, March 1962, pp. 388-396.

[10] Zelenik, F. J. and Gordon, S., "A General Computer Program for Computation of Chemical Equilibrium Compositions . . .," TND-T454, 1962, NASA.

[11] Smoot, L. D., Simonsen, J. M., and Williams, G. A., "Exhaust Plume Prediction Model for a Low-Altitude, Supersonic Missile," AIAA Paper 72-1170, New Orleans, La., 1972.

[12] Mikatarian, R. R. and Pergament, H. S., "Effects of Altitude on Radar Attenuation in Nonequilibrium Afterburning Rocket Exhaust Plumes," *AIAA Journal,* Vol. 7, Jan. 1969, pp. 159-161.